Electrified Au Nanoparticle Sponges with Controlled Hydrophilic/Hydrophobic Properties

Dora Balogh, Ran Tel-Vered, Michael Riskin, Ron Orbach, and Itamar Willner*

Institute of Chemistry and The Center for Nanoscience and Nanotechnology, The Hebrew University of Jerusalem, Jerusalem 91904, Israel

The control of the hydrophilic/hydrophobic properties of surfaces attracts growing interest not only as a means to mimic biological systems[1,2] (e.g., the "lotus effect")[3] but also due to its implementation in practical applications.[4−14] For example, surfaces of controlled wettability were used for the controlled transfer of fluids,[15] in the patterning of surfaces with cells,[16] and for the prevention of biofouling[17] or corrosion.[18] The signal-triggered control of the hydrophilic/hydrophobic properties of surfaces was demonstrated by electrical[19−23] or photochemical[24−28] means. For example, the electrochemically driven shuttling of a hydrophilic rotaxane on a hydrophobic wire led to the control of the hydrophilic/hydrophobic properties of the surface.[29] Also, the potential-induced bending of a long-chain carboxylate monolayer was reported to switch the surface properties between hydrophilic and hydrophobic states.[30] Similarly, photoisomerizable monolayers, such as azobenzene monolayers, demonstrated the reversible photostimulated transition between a hydrophobic state (*trans*-azobenzene) and a state of enhanced hydrophilicity (*cis*-azobenzene).[31]

Recently, we reported on a generic method to imprint molecular recognition sites into Au nanoparticle (NP) composites through the electropolymerization of thioaniline-functionalized Au NPs on Au surfaces and the formation of bisaniline-cross-linked Au NP matrices.[32] According to this method, the electropolymerization of the Au NP composite onto the Au surfaces was conducted in the presence of acceptor substrates that form π-donor−acceptor complexes with the thioaniline and the bisaniline electron donor unit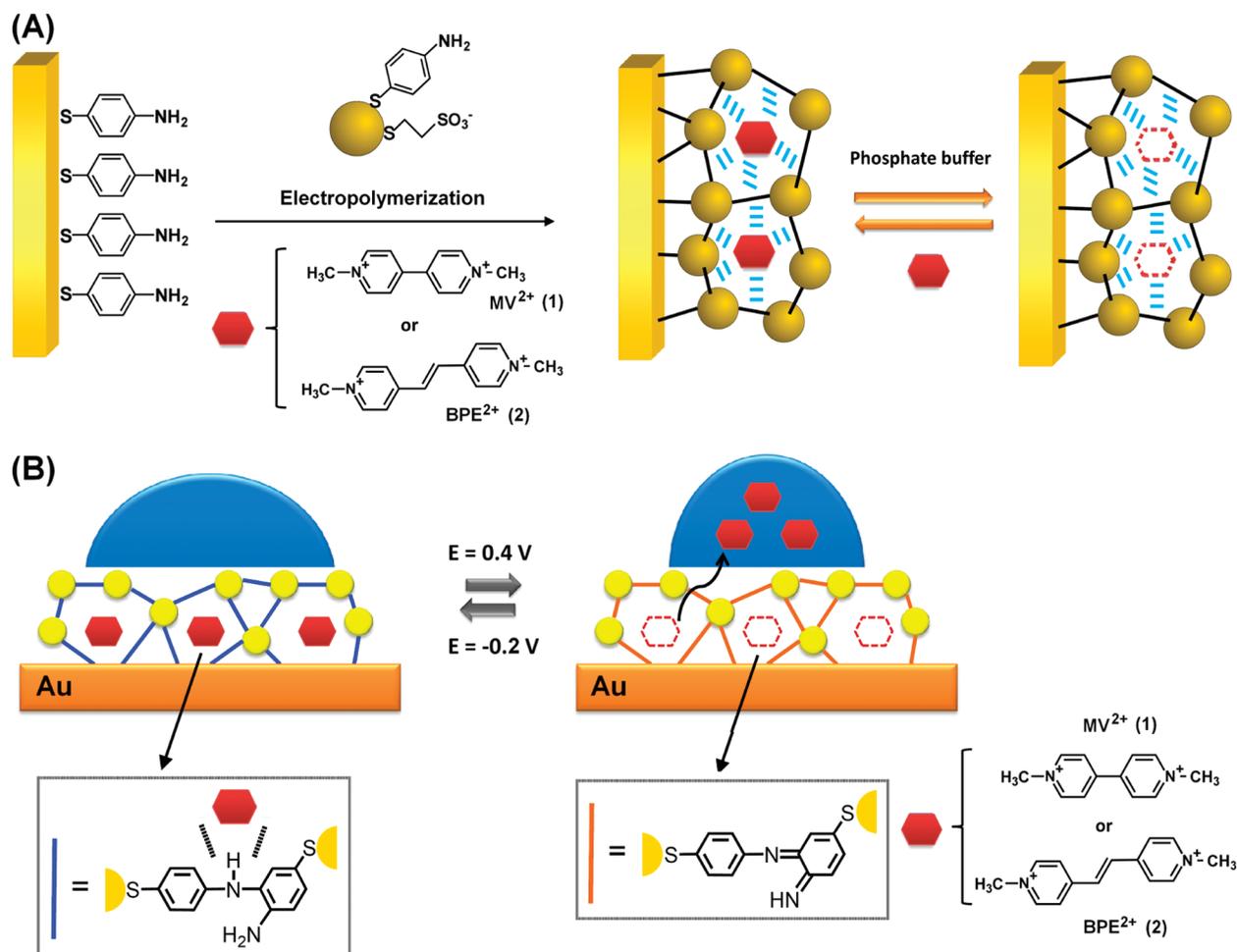s. The subsequent elimination of the acceptor molecules led to the formation of imprinted recognition sites for the imprint molecules, or their analogues, in the resulting Au NP composites. This method was used to generate ultrasensitive and selective sensing matrices for explosives[32−34] and to develop electrochemically triggered Au NP "sponges" for the electrochemically controlled uptake and release of substrates.[35] Here we report on the use of the molecularly imprinted Au NP composites as functional matrices for the electrochemical control of the hydrophilic/hydrophobic properties of surfaces. We demonstrate that the imprinting process at the Au NP composites is essential to yield an interface with controllable wettability and show that this wettability is regulated by the selective binding of the imprinted substrates.

ABSTRACT Molecularly imprinted Au nanoparticle (NP) composites for the selective binding of the electron acceptors *N,N*′-dimethyl-4,4′-bipyridinium, MV^{2+} (1), or bis-*N*-methylpyridinium-4,4′-ethylene, BPE^{2+} (2), are prepared by the electropolymerization of thioaniline-functionalized Au NPs in the presence of the electron acceptor molecules and the subsequent rinsing off of the imprint substrates. The electrochemical oxidation of the π-donor bisaniline units bridging the Au NPs yields the quinoid electron acceptor bridges, which are re-reduced to the bisaniline state. By the cyclic oxidation and reduction of the bridging units, they are reversibly switched between the π-acceptor and the π-donor states, thus allowing the electrochemically triggered uptake and release of the electron acceptors (1 or 2) to and from the imprinted sites. While the electron acceptors 1 or 2 bind to the imprinted sites *via* donor−acceptor interactions, these substrates are released from the Au NP matrices upon the oxidation of the bridges to the quinoid state. The electrochemically switched wettability of the imprinted composites is demonstrated upon the reversible uptake, or release, of the substrates to and from the matrices. While the association of 1 or 2 to the respectively imprinted composites generates hydrophilic surfaces (θ = 30 and 41°, respectively), the release of the substrates from the matrices yields surfaces of enhanced hydrophobicity (θ = 60 and 55°, respectively). The electrochemically switched wettability is selective to the imprinted substrates and is amplified in the presence of the imprinted matrices as compared to the non-imprinted composites. The association of MV^{2+} or BPE^{2+} to the imprinted sites is further electrochemically characterized.

KEYWORDS: Au nanoparticles · electropolymerization · molecular imprinting · wettability · electrochemical switch

Scheme 1. (A) Schematic presentation of the electropolymerization of the bisaniline-cross-linked Au NP composite and the imprinting of the π-acceptor molecules N,N′-dimethyl-4,4′-bipyridinium, MV^{2+} (1), and N,N′-dimethylbipyridinium-4,4′-ethylene dichloride, BPE^{2+} (2). (B) Electrostimulated wettability changes by the uptake and release of π-acceptor molecules using the imprinted bisaniline-cross-linked Au NP composite.

RESULTS AND DISCUSSION

Two electron acceptors, N,N′-dimethyl-4,4′-bipyridinium, MV^{2+} (1), or bis-N-methylpyridinium-4,4′-ethylene, BPE^{2+} (2), were imprinted in the Au NP composite (Scheme 1A). Au NPs (diameter ca. 3.5 nm) functionalized with a mixed capping monolayer consisting of mercaptoaniline and mercaptoethane sulfonic acid were electropolymerized onto a thioaniline-functionalized Au surface in the presence of the electron acceptors 1 or 2. The formation of π-donor–acceptor complexes between the 1 or 2 electron acceptors and the thioaniline or the electropolymerized bisaniline units led to the incorporation of 1 or 2 into the composite. The subsequent rinsing off of 1 or 2 from the Au NP composites yielded the imprinted sites. Similarly, electropolymerized bisaniline-cross-linked Au NP matrices were prepared in the absence of 1 or 2 to yield the non-imprinted Au NP composite. The AFM image of the resulting Au NP film reveals a rough surface with an average height of ca. 30 nm that includes aggregated spikes as high as 60−80 nm (see Supporting Information, Figure S1). The bisaniline bridging units,

cross-linking the Au NPs in the composite, exhibit quasi-reversible redox features, $E^{\circ\prime} = 0.1$ V versus Ag quasi-reference electrode (Ag QRE) at pH 7.4, that enable the transformation of the bisaniline π-donor units into the quinoid π-acceptor state. Thus, the binding of the π-acceptor substrates MV^{2+} or BPE^{2+} to the cross-linked Au NPs is expected to be electroswitchable. While the bisaniline donor sites bind the electron acceptors by π-donor–acceptor interactions, the electro-oxidation of the bridging units to the quinoid acceptor state should release the acceptor substrates from the matrices (Scheme 1B).

We find that the electrochemically induced uptake and release of the electron acceptors, MV^{2+} or BPE^{2+}, to and from the imprinted bisaniline-cross-linked Au NP composite controls the hydrophilic/hydrophobic properties of the surface. The association of the electron acceptor MV^{2+} (1) to the bisaniline donor bridges yields a hydrophilic surface (Figure 1A, image I (contact angle for the MV^{2+} solution droplet, $\theta = 30°$)), whereas the oxidation of the cross-linking units to the quinoid state leads to the release of the electron acceptor MV^{2+} to the
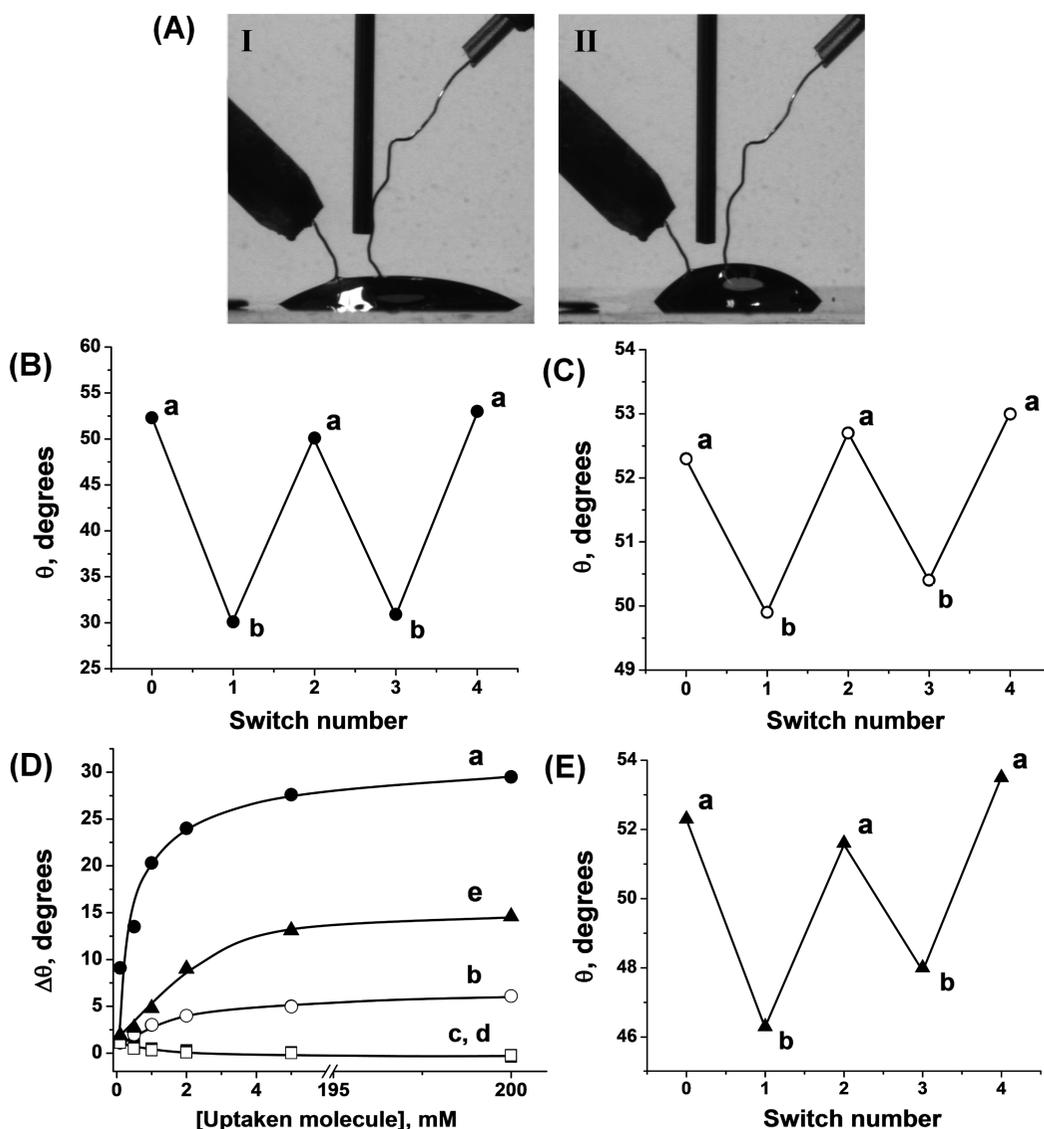
Figure 1. (A) Images showing changes in the contact angle for a droplet containing MV^{2+}, 1 mM, on the MV^{2+}-imprinted bisaniline-cross-linked Au NP electrode, upon the application of (I) a reductive potential pulse, $E = -0.2$ V (vs Ag QRE), for 10 min, (II) an oxidative potential pulse, $E = 0.4$ V, for 10 min. (B) Cyclic electrical switching of the contact angle of the droplet in (A) by the application of (a) $E = 0.4$ V for 10 min, and (b) $E = -0.2$ V for 10 min. (C) Similar measurement as in (B), for the non-imprinted matrix. (D) Contact angle changes recorded in the presence of different concentrations of the imprint molecules: (a) MV^{2+}-imprinted Au NP composite in the presence of MV^{2+}, upon the application of $E = -0.2$ V for 10 min; (b) non-imprinted Au NP composite in the presence of MV^{2+}, upon the application of $E = -0.2$ V for 10 min; (c) same as in (a), upon the application of $E = 0.4$ V for 10 min; (d) same as in (b), upon the application of $E = 0.4$ V for 10 min; (e) MV^{2+}-imprinted Au NP composite in the presence of BPE^{2+}, upon the application of $E = -0.2$ V for 10 min. (E) Same as in (B), for a BPE^{2+} droplet, 1 mM. $\Delta\theta$ corresponds to the difference between the contact angle of the composite modified surface before and after the addition of the respective concentration of the electron acceptor.

solution and to the formation of a surface exhibiting enhanced hydrophobicity, $\theta = 55°$ (Figure 1A, image II). By the cyclic electrochemical transformation of the bridging units between the reduced bisaniline and the oxidized quinoid states of the bridges, the surface is cycled between hydrophilic and hydrophobic states, respectively (Figure 1B). While the contact angles of the droplet associated with the MV^{2+}-imprinted Au NP composite differ substantially upon the electrochemical switching of the redox state of the bridging units in the presence of MV^{2+} (ca. $\Delta\theta = 23°$ between the reduced and oxidized states), the non-imprinted Au NP

composite shows only small differences in the contact angle of the droplet, $\Delta\theta = 2°$ (Figure 1C). This is consistent with the fact that the association of MV^{2+} to the imprinted sites reveals high affinity, leading to the high loading of the "sponge" with the hydrophilic MV^{2+} (**1**). The substantial lower affinity of MV^{2+} for the non-imprinted Au NP matrix leads to the lower loading of the matrix with this substance and to significantly smaller changes in the hydrophilic properties of the surface (for the quantitative assessment of the loading of the different matrices with MV^{2+}, vide infra). It should be noted that the imprinted or non-imprinted bisaniline-

cross-linked Au NP surfaces reveal, in the absence of MV^{2+}, a similar contact angle corresponding to $\theta = 53°$, and the oxidation of the bridging units to the quinoid state leads only to a minute change in the contact angle, $\Delta\theta = 1°$. These control experiments imply that the association of MV^{2+} to the imprinted donor sites is the origin for the switchable wettability properties of the surface.

Figure 1D, curve a, depicts the contact angle changes of the bisaniline-cross-linked Au NP composite in the presence of variable concentrations of MV^{2+} and under an applied potential of $E = -0.2$ V (vs Ag QRE). Evidently, as the concentration of MV^{2+} increases, the hydrophilicity of the surface is enhanced (lower contact angles). For comparison, Figure 1D, curve b, shows the contact angle changes of the imprinted Au NP composite under an applied potential of $E = 0.4$ V and in the presence of variable concentrations of MV^{2+}. The contact angle changes are small, $\Delta\theta = 5°$, implying that MV^{2+} does not bind strongly to the matrix when the bridges are in the oxidized quinoid form. Figure 1D, curve c, shows the contact angle changes of the non-imprinted Au NP composite under an applied potential of $E = -0.2$ V in the presence of variable concentrations of MV^{2+}. The contact angle changes are very small, consistent with the low loading of the non-imprinted matrix with MV^{2+}. Also, the non-imprinted Au NP composite, subjected to an oxidative potential, $E = 0.4$ V, where the bridging units lack an affinity for MV^{2+}, does not show any contact angle changes upon interaction with variable concentrations of MV^{2+} (Figure 1D, curve d). A major aspect to consider relates, however, to the selectivity of the imprinted sites and, thus, to the possibility to selectively control the hydrophilicity of the surface. Toward this goal, the MV^{2+}-imprinted Au NP composite was interacted with variable concentrations of bis-N,N'-dimethylpyridinium, 4,4'-ethylene, BPE^{2+} (2), under an applied potential of $E = -0.2$ V, where the bridging units exist in their reduced π-donor state (Figure 1D, curve e). Substantially lower contact angle changes, as compared to the changes with MV^{2+}, are observed, implying a lower affinity of BPE^{2+} to the imprinted sites. Figure 1E shows the cyclic contact angle changes observed on the MV^{2+}-imprinted Au NP composite upon treatment with 1 mM BPE^{2+} and by cycling the potential between $E = -0.2$ V (keeping the bridging units in their reduced state) and $E = 0.4$ V (retaining the bridging units in their oxidized quinoid state). Small contact angle changes (ca. $\Delta\theta = 5°$) are observed, consistent with the inefficient uptake of BPE^{2+} by the MV^{2+}-imprinted matrix.

We further elucidated, by chronoamperometric measurements, the content of MV^{2+} associated with the MV^{2+}-imprinted and the non-imprinted Au NP composites. Assuming that the leakage of MV^{2+} from the different composites is slow during the rapid chronoamperometric experiments, the imprinted or non-imprinted Au NP composites were challenged with different concentrations of MV^{2+}, and the resulting

equilibrated electrodes were subjected to a reduction potential step from $E = -0.4$ V to $E = -0.8$ V versus Ag QRE ($E°_{MV^{2+}/MV^+} = -0.65$ V vs Ag QRE). The transient current generated upon the reduction of the surface-confined MV^{2+} is given by eq 1, where k_{et} is the electron transfer rate constant and Q is the charge associated with the redox process.[36,37] In fact, this relation was used in the past to elucidate the coverage of surface-confined redox compounds.

$$I(t) = Qk_{et}e^{-k_{et}t} \tag{1}$$

Figure 2A depicts a typical chronoamperometric current transient that was recorded for the MV^{2+}-imprinted Au NP composite-modified electrode interacted with a
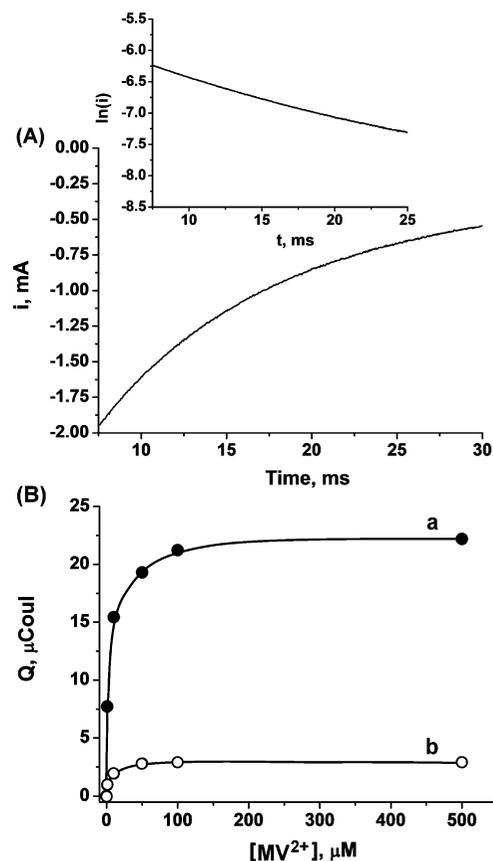

Figure 2. (A) Chronoamperometric transient corresponding to the reduction of MV^{2+} on the MV^{2+}-imprinted bisaniline-cross-linked Au NP composite-modified electrode, following the application of a potential step from $E = -0.4$ V to $E = -0.8$ V (vs Ag QRE). The electrode was pretreated with MV^{2+}, 5×10^{-4} M, for 10 min. The measurement was performed in a phosphate buffer (0.1 M, pH 7.2). Inset: Linear correlation between the natural logarithm of the current and the duration of the potential pulse, from which the charge associated with the MV^{2+} species was evaluated. (B) Coulometric analysis corresponding to the application of a potential step from $E = -0.4$ V to $E = -0.8$ V on (a) MV^{2+}-imprinted bisaniline-cross-linked Au NP composite-modified electrode and (b) non-imprinted bisaniline-cross-linked Au NP composite-modified electrode, upon the pretreatment of the electrodes with different concentrations of MV^{2+} for 10 min. The measurements were performed in a phosphate buffer solution (0.1 M, pH 7.2) purged with N_2 for 15 min. During the measurements, a stream of N_2 was kept above the electrolyte.
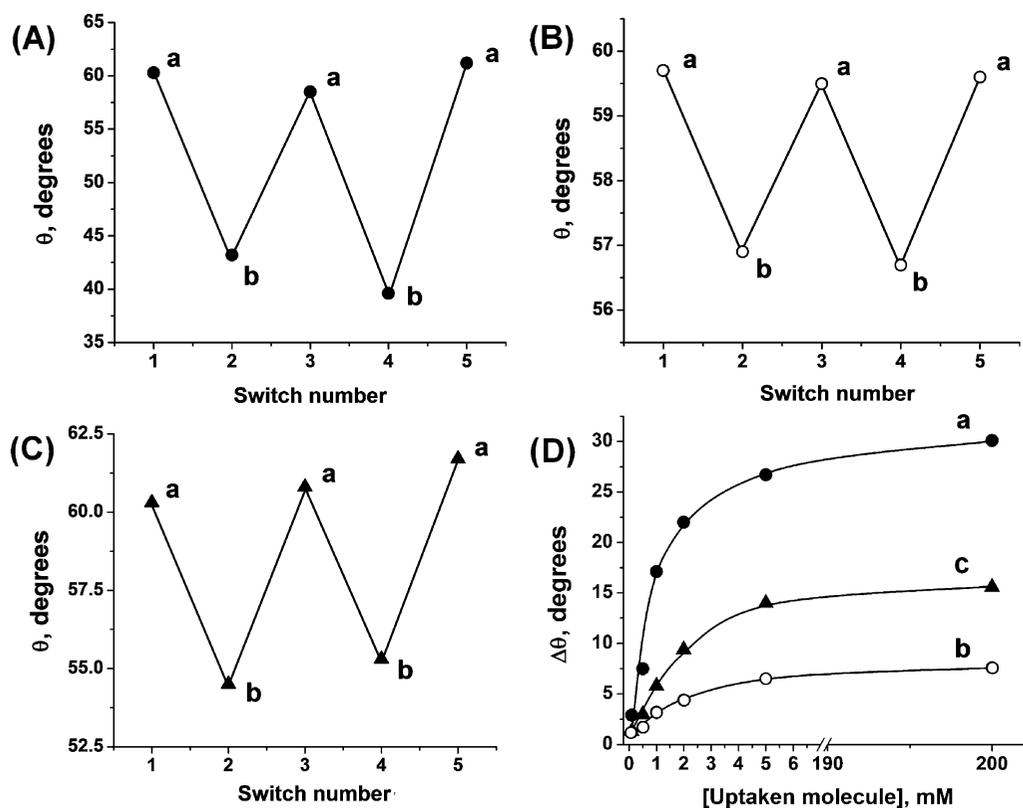
Figure 3. (A) Cyclic electrical switching of the contact angle for a droplet containing 1 mM BPE^{2+} on the BPE^{2+}-imprinted bisaniline-cross-linked Au NP composite-modified electrode by the repetitive application of the potential pulses: (a) $E = 0.4$ V (*vs* Ag QRE) for 10 min and (b) $E = -0.2$ V for 10 min. (B) Same as in (A) for the non-imprinted bisaniline-cross-linked Au NP composite-modified electrode. (C) Cyclic contact angle switching for a droplet containing 1 mM MV^{2+} on the BPE^{2+}-imprinted bisaniline-cross-linked Au NP composite-modified electrode. (D) Contact angle changes recorded in the presence of different concentrations of the imprint molecules: (a) BPE^{2+}-imprinted Au NP composite in the presence of BPE^{2+}; (b) non-imprinted Au NP composite in the presence of BPE^{2+}; (c) BPE^{2+}-imprinted Au NP composite in the presence of MV^{2+}. All measurements were performed upon the application of $E = -0.2$ V on the electrodes for 10 min. $\Delta\theta$ corresponds to the difference between the contact angle of the composite modified surface before and after the addition of the respective concentration of the electron acceptor.

bulk concentration of MV^{2+} corresponding to 5×10^{-4} M. Figure 2A, inset, shows the semilogarithmic analysis of the current transient according to eq 1, from which the values of $k_{et} = 60$ s^{-1} and $Q = 2.2 \times 10^{-5}$ coulombs (surface coverage of *ca*. 2.3×10^{-10} mol cm^{-2}) are derived. Figure 2B, curve a, shows the curve corresponding to the charge associated with the MV^{2+}-imprinted Au NP matrix challenged with different bulk concentrations of MV^{2+}. The charge associated with the electrode increases as the bulk concentration of MV^{2+} is elevated, and it levels off at a concentration of 5×10^{-4} M, consistent with the saturation of the imprinted sites. Using a Langmuir-type binding of MV^{2+} to the imprinted sites, the derived association constant of MV^{2+} to the MV^{2+}-imprinted Au NP matrix corresponds to $K_a = 5.0 \times 10^5$ M^{-1} (for the determination of the association constants, see Supporting Information). For comparison, similar chronoamperometric measurements were performed on the non-imprinted Au NP composite. Figure 2B, curve b, shows the charge associated with the binding of MV^{2+} to the non-imprinted matrix. The derived association constant corresponds to $K_a = 8.3 \times 10^4$ M^{-1}, a value that is *ca*. 6-fold lower than the association constant of MV^{2+} to the MV^{2+}-

imprinted Au NP composite. These results reveal that the binding of MV^{2+} to the MV^{2+}-imprinted Au NP aggregate leads to the formation of high affinity binding sites for the electron acceptor substrate.

We, then, examined the possibility to imprint specific molecular recognition sites for BPE^{2+} into the Au NP matrix and to selectively control the wettability of the surface by means of the BPE^{2+} electron acceptor. The BPE^{2+}-imprinted bisaniline-cross-linked Au NP composite was prepared by the electropolymerization of the thioaniline-modified Au NPs in the presence of BPE^{2+}, followed by rinsing off of the imprint molecule. Figure 3A shows the contact angle changes upon switching the potential on an electrode modified with the BPE^{2+}-imprinted Au NP composite in the presence of 1 mM BPE^{2+}. At the negative potential, $E = -0.2$ V, where the bridging units exist in their reduced bisaniline π-donor state, the surface reveals hydrophilic properties, average contact angle $\theta = 41°$, consistent with the binding of the positively charged BPE^{2+} to the matrix by donor–acceptor interactions. The electrochemical oxidation of the bridging units to the quinoid state releases the BPE^{2+} from the composite, resulting in a surface of lower hydrophilicity, average contact

angle $\theta = 60°$. By the reversible switching of the potential applied on the electrode between the negative and the positive values, the wettability properties of the surface are switched between the hydrophilic and hydrophobic states, respectively. For comparison, Figure 3B shows the contact angle changes upon switching the potential on the non-imprinted Au NP-modified electrode, in the presence of 1 mM BPE^{2+}. Only small contact angle changes are observed, $\Delta\theta = 2.5°$, implying a low concentration of BPE^{2+} associated with the non-imprinted matrix. Furthermore, Figure 3C depicts the contact angle changes upon the switching of the potential on the BPE^{2+}-imprinted Au NP composite, in the presence of 1 mM MV^{2+}. The contact angle changes, $\Delta\theta = 6°$, are substantially lower than those in the presence of BPE^{2+} and, also, significantly smaller than the contact angle changes observed in the presence of MV^{2+} on the MV^{2+}-imprinted Au NP composite. These results imply that the imprinting process leads to the generation of selective recognition sites. That is, the imprinting of BPE^{2+} yields high affinity binding sites for BPE^{2+} with low affinity toward the association of MV^{2+}. Also, the high affinity of the bisaniline-cross-linked Au NP matrix for BPE^{2+} leads to the high loading of the matrix with the imprinted substrate. Figure 3D, curve a, shows the contact angle changes of the BPE^{2+}-imprinted bisaniline-cross-linked Au NP composite at $E = -0.2$ V in the presence of variable concentrations of BPE^{2+}. As the concentration of BPE^{2+} increases, the contact angle changes intensify, indicating that the surface turns more hydrophilic. Figure 3D, curve b, shows the contact angle changes of the non-imprinted bisaniline-cross-linked Au NP composite, in the presence of variable concentrations of BPE^{2+} at $E = -0.2$ V. Small changes in the contact angle values are observed, demonstrating that BPE^{2+} exhibits low affinity and, thus, low loading for the association to the non-imprinted composite. Also, Figure 3D, curve c, depicts the contact angle changes of the BPE^{2+}-imprinted Au NP composite at $E = -0.2$ V in the presence of variable concentrations of MV^{2+}. Only small contact angle changes are observed, demonstrating that the imprinted Au NPs matrix reveals selectivity and that MV^{2+} has a low affinity for the BPE^{2+}-imprinted sites.

The qualitative assays of the loading of the BPE^{2+} on the BPE^{2+}-imprinted and non-imprinted Au NP composites, at different bulk concentrations of BPE^{2+}, were assessed by chronoamperometric experiments. Figure 4, curve a, depicts the calibration curve corresponding to the coulometric analysis of the redox wave of BPE^{2+} generated following the pretreatment of the electrode with different bulk concentrations of BPE^{2+}. To this end,
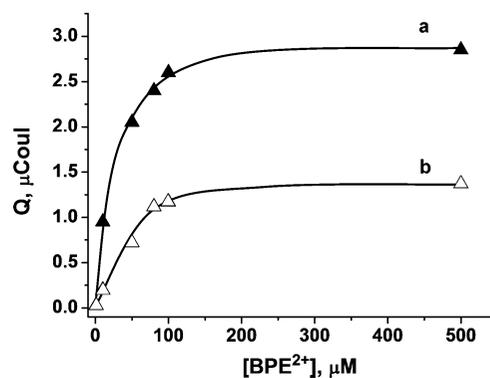

Figure 4. Coulometric analysis corresponding to the application of a potential step from $E = -0.2$ V to $E = -0.5$ V (vs Ag QRE) on (a) BPE^{2+}-imprinted bisaniline-cross-linked Au NP composite-modified electrode and (b) non-imprinted bisaniline-cross-linked Au NP composite-modified electrode, upon the pretreatment of the electrodes with different concentrations of BPE^{2+} for 10 min. The measurements were performed in a phosphate buffer solution (0.1 M, pH 7.2) purged with N$_2$ for 15 min. During the measurements, a stream of N$_2$ was kept above the electrolyte level.

the potential was stepped from $E = -0.2$ V to $E = -0.5$ V versus Ag QRE ($E°_{BPE^{2+}/BPE^+} = -0.35$ V vs Ag QRE). Using the Langmuir model, the association constant for binding BPE^{2+} to the imprinted matrix was estimated to be $K_a = 1.4 \times 10^5$ M^{-1}. Figure 4, curve b, shows the derived coulometric calibration curve corresponding to the association of BPE^{2+} to the non-imprinted bisaniline-cross-linked Au NP composite, showing that a substantially lower content of BPE^{2+} is associated with the non-imprinted matrix, with an estimated association constant of $K_a = 4.5 \times 10^4$ M^{-1}.

In conclusion, the present study has demonstrated the electrochemical control of the hydrophilic/hydrophobic properties of bisaniline-cross-linked Au NP composites via the uptake or release of the hydrophilic electron acceptors, MV^{2+} or BPE^{2+}, to and from the matrices. We demonstrated the control of the bisaniline-cross-linked Au NP composites by the imprinting procedure that led to the generation of high affinity binding sites for the imprinted substrates MV^{2+} or BPE^{2+}, allowing an effective association of the imprint molecules to the corresponding matrices. Furthermore, we highlighted that the imprinting process leads to the selective control of the hydrophilic/hydrophobic properties of the surface. That is, under the application of an external voltage trigger, the MV^{2+}- or BPE^{2+}-imprinted Au NP matrices result, in the presence of the respective imprint molecule, in electrochemically induced hydrophilic/hydrophobic surfaces.

METHODS

Nanoparticles Synthesis. Au nanoparticles functionalized with 2-mercaptoethane sulfonic acid and *p*-aminothiophenol (Au NPs) were prepared by mixing a 10 mL solution containing 197 mg of HAuCl$_4$ in methanol and a 5 mL solution containing 42 mg

of mercaptoethane sulfonate and 8 mg of *p*-aminothiophenol in methanol. The two solutions were stirred in the presence of 2.5 mL of glacial acetic acid in an ice bath for 1 h. Subsequently, 7.5 mL of an aqueous solution of 1 M sodium borhydride, NaBH$_4$, was added dropwise, resulting in a dark color solution associ-

ated with the presence of the Au NPs. The solution was stirred for 1 additional hour in an ice bath and then for 14 h at room temperature. The particles were successively washed and centrifuged (twice in each solvent) with methanol, ethanol, and diethyl ether. A mean particle size of *ca.* 3.5 nm was estimated using TEM.

Modification of the Electrodes. *p*-Aminothiophenol-functionalized electrodes were prepared by immersing the Au slides for 24 h into a 50 mM *p*-aminothiophenol ethanolic solution. In order to prepare the bisaniline-cross-linked Au NP composite on the electrode, the surface-tethered *p*-aminothiophenol groups were electropolymerized in a 0.1 M HEPES solution (pH 7.2) containing 2 mg mL^{-1} of *p*-aminothiophenol-functionalized Au NPs. The polymerization was performed by the application of 80 potential cycles between $E = -0.3$ and $E = 0.8$ V *versus* a KCl-saturated calomel electrode (SCE) at a potential scan rate of 100 mV s^{-1}. The resulting films were, then, washed with the background buffer solution to exclude any residual monomer from the electrode. Similarly, imprinted bisaniline-cross-linked films were prepared by adding 10 mM of the imprint molecule to the Au NP mixture prior to the electropolymerization process. The extraction of the imprint molecules from the film was carried out by immersing the electrodes overnight in a phosphate buffer solution (0.1 M, pH 7.4) at room temperature.

Instrumentation. Static contact angle measurements were performed on the modified Au surface by using a CAM 2000 Optical-Angle Analyzer (KSV Instruments, Finland). A droplet of the phosphate buffer solution (0.1 M, pH 7.4), approximately 20 μL with diameter of roughly 0.5 cm, was deposited on the surface by using a syringe. The images of the droplets were recorded, and each contact angle measurement was repeated at least five times. The reported values represent the average of these results. Electrochemical measurements were performed using a PC-controlled (Autolab GPES software) potentiostat/galvanostat (μAutolab, type III). In these measurements, a graphite rod (*d* = 5 mm) was used as the counter electrode. AFM imaging was performed at room temperature using a multimode scanning probe microscope with a Nanoscope 3A controller (Digital Instruments, Veeco Probes, USA). The image was taken with a NSC 15 AFM tip (Mikromasch, Germany) using the tapping mode at its resonant frequency. The image was analyzed with a WsXM SPIP software (Nanotec, Inc., Spain).

Supporting Information Available: AFM image of the bisaniline-cross-linked Au NP-modified Au surface and the derivation of the association constants using the Langmuir model are provided. This material is available free of charge *via* the Internet at http://pubs.acs.org.

REFERENCES AND NOTES

1. Fogg, G. E. Diurnal Fluctuation in a Physical Property of Leaf Cuticle. *Nature* **1944**, *154*, 515.
2. Cassie, A. B. D.; Baxter, S. Large Contact Angles of Plant and Animal Surfaces. *Nature* **1945**, *155*, 21–22.
3. Barthlott, W.; Neinhuis, C. Purity of Sacred Lotus, or Escape from Contamination in Biological Surfaces. *Planta* **1997**, *202*, 1–8.
4. Zhang, X.; Shi, F.; Niu, J.; Jiang, Y. G.; Wang, Z. Q. Superhydrophobic Surfaces: From Structural Control to Functional Application. *J. Mater. Chem.* **2008**, *18*, 621–633.
5. Roach, P.; Shirtcliffe, N. J.; Newton, M. I. Progress in Superhydrophobic Surface Development. *Soft Matter* **2008**, *4*, 224–240.
6. Li, X. M.; Reinhoudt, D.; Crego-Calama, M. What Do We Need for Superhydrophobic Surface? A Review on the Recent Progress in the Preparation of Superhydrophobic Surfaces. *Chem. Soc. Rev.* **2007**, *36*, 1350–1368.
7. Feng, X. J.; Jiang, L. Design and Creation of Superwetting/Antiwetting Surfaces. *Adv. Mater.* **2006**, *18*, 3063–3078.
8. Ma, M. L.; Hill, R. M. Superhydrophobic Surfaces. *Curr. Opin. Colloid Interface Sci.* **2006**, *11*, 193–202.
9. Sun, T. L.; Feng, L.; Gao, X. F.; Jiang, L. Bioinspired Surfaces with Special Wettability. *Acc. Chem. Res.* **2005**, *38*, 644–652.
10. Nath, N.; Chilkoti, A. Creating "Smart" Surfaces Using Stimuli Responsive Polymers. *Adv. Mater.* **2002**, *14*, 1243–1247.
11. Liu, H.; Zhai, J.; Jiang, L. Wetting and Anti-wetting on Aligned Carbon Nanotube Films. *Soft Matter* **2006**, *2*, 811–821.
12. Feng, X. J.; Feng, L.; Jin, M. H.; Zhai, J.; Jiang, L.; Zhu, D. B. Reversible Super-Hydrophobicity to Super-Hydrophilicity Transition of Aligned ZnO Nanorod Films. *J. Am. Chem. Soc.* **2004**, *126*, 62–63.
13. Wang, R.; Hashimoto, K.; Fujishima, A.; Chikuni, M.; Kojima, E.; Kitamura, A.; Shimohigoshi, M.; Watanabe, T. Light-Induced Amphiphilic Surfaces. *Nature* **1997**, *388*, 431–432.
14. Sun, T. L.; Wang, G. J.; Feng, L.; Liu, B. Q.; Ma, Y. M.; Jiang, L.; Zhu, D. B. Reversible Switching between Superhydrophilicity and Superhydrophobicity. *Angew. Chem., Int. Ed.* **2004**, *43*, 357–360.
15. Pollack, M. G.; Fair, R. B.; Shendrov, A. D. Electrowetting-Based Actuation of Liquid Droplets for Microfluidic Applications. *Appl. Phys. Lett.* **2000**, *77*, 1725–1726.
16. Ostuni, E.; Chen, C. S.; Ingber, D. E.; Whitesides, G. M. Selctive Deposition of Proteins and Cells in Arrays of Microwells. *Langmuir* **2001**, *17*, 2828–2834.
17. Zhang, H.; Lamba, R.; Lewis, J. Engineering Nanoscale Roughness on Hydrophobic Surface—Preliminary Assessment of Fouling Behavior. *Sci. Technol. Adv. Mater.* **2005**, *6*, 236–239.
18. Liu, T.; Yin, Y. S.; Chen, S. G.; Chang, X. T.; Cheng, S. Super-Hydrophobic Surfaces Improve Corrosion Resistance of Copper in Seawater. *Electrochim. Acta* **2007**, *52*, 3709–3713.
19. Riskin, M.; Basnar, B.; Chegel, V. I.; Katz, E.; Willner, I.; Shi, F.; Zhang, X. Switchable Surface Properties through the Electrochemical or Biocatalytic Generation of Ag^0 Nanoclusters on Monolayer-Functionalized Electrodes. *J. Am. Chem. Soc.* **2006**, *128*, 1253–1260.
20. Riskin, M.; Basnar, B.; Katz, E.; Willner, I. Cyclic Control of the Surface Properties of a Monolayer-Functionalized Electrode by the Electrochemical Generation of Hg Nanoclusters. *Chem.—Eur. J.* **2006**, *12*, 8549–8557.
21. Wang, X. M.; Kharitonov, A. B.; Katz, E.; Willner, I. Potential-Controlled Molecular Machinery of Bipyridinium Monolayer-Functionalized Surfaces: an Electrochemical and Contact Angle Analysis. *Chem. Commun.* **2003**, 1542–1543.
22. Mu, L.; Liu, Y.; Cai, S. Y.; Kong, J. L. A Smart Surface in a Microfluidic Chip for Controlled Protein Separation. *Chem.—Eur. J.* **2007**, *13*, 5113–5120.
23. Abbott, N. L.; Gorman, C. B.; Whitesides, G. M. Active Control of Wetting Using Applied Electrical Potentials and Self-Assembled Monolayers. *Langmuir* **1995**, *11*, 16–18.
24. Oh, S. K.; Nakagawa, M.; Ichimura, K. Photocontrol of Liquid Motion on an Azobenzene Monolayer. *J. Mater. Chem.* **2002**, *12*, 2262–2269.
25. Driscoll, P. F.; Purohit, N.; Wanichacheva, N.; Lambert, C. R.; McGimpsey, W. G. Reversible Photoswitchable Wettability in Noncovalently Assembled Multilayered Films. *Langmuir* **2007**, *23*, 13181–13187.
26. Vlassiouk, I.; Park, C. D.; Vail, S. A.; Gust, D.; Smirnov, S. Control of Nanopore Wetting by a Photochromic Spiropyran: A Light-Controlled Valve and Electrical Switch. *Nano Lett.* **2006**, *6*, 1013–1017.
27. Doron, A.; Katz, E.; Tao, G. L.; Willner, I. Photochemically-, Chemically-, and pH-Controlled Electrochemistry at Functionalized Spiropyran Monolayer Electrodes. *Langmiur* **1997**, *13*, 1783–1790.
28. Riskin, M.; Katz, E.; Gutkin, V.; Willner, I. Photochemically Controlled Electrochemical Deposition and Dissolution of Ag^0 Nanoclusters on Au Electrode Surfaces. *Langmuir* **2006**, *22*, 10483–10489.
29. Katz, E.; Lioubashevsky, O.; Willner, I. Electromechanics of a Redox-Active Rotaxane in a Monolayer Assembly on an Electrode. *J. Am. Chem. Soc.* **2004**, *126*, 15520–15532.

30. Lahann, J.; Mitragotri, S.; Tran, T.-N.; Kaido, H.; Sundara, J.; Choi, I. S.; Hoffer, S.; Somorjai, G. A.; Langer, R. A Reversibly Switching Surface. *Science* **2003**, *299*, 371–374.

31. Ichimura, K.; Oh, S. K.; Nakagawa, M. Light-Driven Motion of Liquids on a Photoresponsive Surface. *Science* **2000**, *288*, 1624–1626.

32. Riskin, M.; Tel-Vered, R.; Bourenko, T.; Granot, E.; Willner, I. Imprinting of Molecular Recognition Sites through Electropolymerization of Functionalized Au Nanoparticles: Development of an Electrochemical TNT Sensor Based on π-Donor−Acceptor Interactions. *J. Am. Chem. Soc.* **2008**, *130*, 9726–9733.

33. Riskin, M.; Tel-Vered, R.; Lioubashevsky, O.; Willner, I. Ultrasensitive Surface Plasmon Resonance Detection of Trinitrotoluene by a Bis-aniline-Cross-Linked Au Nanoparticles Composite. *J. Am. Chem. Soc.* **2009**, *131*, 7368–7378.

34. Riskin, M.; Tel-Vered, R.; Willner, I. Imprinted Au-Nanoparticle Composites for the Ultrasensitive Surface Plasmon Resonance Detection of Hexahydro-1,3,5-trinitro-1,3,5-triazine (RDX). *Adv. Mater.* **2010**, *22*, 1387–1391.

35. Frasconi, M.; Tel-Vered, R.; Riskin, M.; Willner, I. Electrified Selective "Sponges" Made of Au Nanoparticles. *J. Am. Chem. Soc.* **2010**, *132*, 9373–9382.

36. Finklea, H. O.; Ravenscroft, M. S.; Snider, D. A. Electrolyte and Temperature Effects on Long-Range Electron-Transfer across Self-Assembled Monolayers. *Langmuir* **1993**, *9*, 223–227.

37. Katz, E.; Willner, I. Kinetic Separation of Amperometric Responses of Composite Redox-Active Monolayers Assembled onto Au Electrodes: Implications to the Monolayers' Structure and Composition. *Langmuir* **1997**, *13*, 3364–3373.